nature astronomy

Article

https://doi.org/10.1038/s41550-024-02364-y

Nitrogen-rich organics from comets probed by ultra-carbonaceous Antarctic micrometeorites

Received: 7 July 2023

Accepted: 13 August 2024

Published online: 10 September 2024

Check for updates

J. Rojas[1,2] ✉, J. Duprat[3], E. Dartois[4], T-D. Wu[5], C. Engrand[1], L. R. Nittler[2,6], N. Bardin[1], L. Delauche[1], S. Mostefaoui[3], L. Remusat[3], R. M. Stroud[6,7] & B. Guérin[1]

The nature of the organic matter in interplanetary samples is central to elucidating the formation and early evolution of the Solar System. Although most meteorites derive from asteroids, micrometeorites mainly sample more remote objects. Ultra-carbonaceous Antarctic micrometeorites (UCAMMs), which have the highest carbon content among interplanetary samples, offer a unique window into cometary organics. Here we report a survey of the H, C and N isotopes in four UCAMMs, of which two are ^{15}N-poor ($\delta^{15}N \simeq -120‰$), which suggests that their formation involved primordial N_2 ($\delta^{15}N \simeq -380‰$). Such a composition could be the result of Galactic cosmic ray irradiation of N_2 ices at the surface of cold small bodies in the outermost parts of the Solar System, possibly the Oort cloud. The two other UCAMMs exhibit higher $\delta^{15}N$ (75‰ and 282‰), like those reported for carbonaceous chondrites and interplanetary dust particles. They may originate from parent bodies initially on lower heliocentric orbits in the Kuiper belt that have surfaces cold enough to retain N-bearing species, such as cyanides ($\delta^{15}N \geq 200‰$), that are richer in ^{15}N than primordial N_2. According to their elemental and isotopic composition, UCAMMs constitute a unique probe into the coldest objects of the Solar System, namely those in the Kuiper Belt and the Oort cloud, which are largely out of reach of current space exploration.

The isotopic composition of extraterrestrial samples provides key information about asteroids and comets originating from diverse heliocentric distances. The carbonaceous component of these interplanetary samples mainly consists of organic matter (OM), which is a record of the low-temperature molecular reservoirs that were present in their regions of accretion and the subsequent evolution of their parent bodies. The isotopic signature of the light elements (H, C and N) constitutive of this OM is a powerful tool for comparing the diversity of interplanetary objects and for studying their origin and evolution from the presolar molecular cloud to the disk phase up to their later processing in their parent bodies. Extensive studies have been performed on insoluble organic matter (IOM) extracted from meteorites[1–3], thin sections of meteorites[4–9], interplanetary dust particles[10–16] (IDPs) collected in the stratosphere, samples from the comet 81P/Wild 2 returned by the Stardust mission[17] and, most recently, samples from the surface of the carbonaceous asteroid Ryugu returned by the Hayabusa2 mission[18], which shed light on the complex history and diversity of interplanetary OM. Nonetheless, whether the OM from those objects has a common

[1]Univ. Paris-Saclay, CNRS/IN2P3, IJCLab, Orsay, France. [2]Earth and Planets Laboratory, Carnegie Institution for Science, Washington DC, USA. [3]Muséum National d'Histoire Naturelle, Sorbonne Univ., UMR CNRS 7590, IMPMC, Paris, France. [4]Univ. Paris-Saclay, CNRS, ISMO, Orsay, France. [5]Institut Curie, PSL Univ., Univ. Paris-Saclay, CNRS UAR2016, Inserm US43, Multimodal Imaging Center, Orsay, France. [6]Arizona State University, Tempe, AZ, USA. [7]Naval Research Laboratory, Washington DC, USA. ✉e-mail: jrojas10@carnegiescience.edu

https://doi.org/10.1038/s41550-024-02364-y

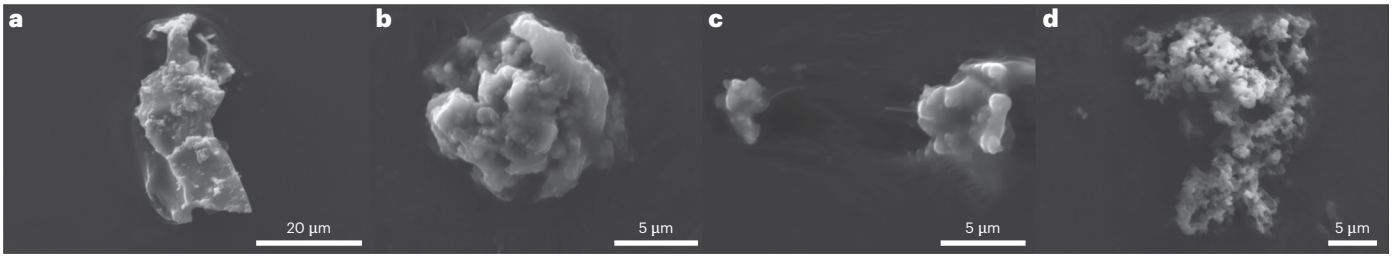

Fig. 1 | Secondary electron images of UCAMM fragments analysed by energy-dispersive X-ray spectrometry. a, DC06-18. **b**, DC06-43. **c**, DC06-94. **d**, DC16-309. Complementary fragments were analysed by NanoSIMS ('Sample analyses' in Methods).

origin or formed in different locations at different times or from different precursors is still a matter of debate. Their nitrogen isotopes are globally enriched in ^{15}N compared to the solar value, which is assumed to reflect the primordial N_2 composition. Of these samples, IDPs and CR chondrites are considered to bear pristine OM with large D and ^{15}N enrichments, which most probably derived from volatile precursors with isotopic fractionations inherited from the presolar molecular cloud or the protoplanetary disk[19,20]. Such precursors are probably still preserved in comets, for which similar enrichments have been reported by remote and in situ sensing[21–23]. Conversely, the limited occurrence of ^{15}N depletion in interplanetary OM indicates that whatever the formation processes of these organics, they only involved marginally the hypervolatile primordial N_2.

In the last 15 years, ultra-carbonaceous Antarctic micrometeorites (UCAMMs)[24–27] have been identified in French and Japanese Antarctic micrometeorite collections[28,29]. These are providing new opportunities to deepen our understanding of the diversity of OM in Solar System objects. Yet, with only nine samples reported to date[24–27], they remain rare and challenging to analyse. These highly carbon-rich particles exhibit minimal terrestrial weathering[25,30]. They are characterized by the highest bulk elemental C/Si ratios (exceeding 10) observed in interplanetary objects[27,30]. The mineralogical, chemical and isotopic composition of UCAMMs indicates that they most probably originated from the surface of icy parent bodies[26,27]. However, light-element isotopic data on the OM in UCAMMs remain scarce. Extreme D/H ratios have been reported for two UCAMMs from the Concordia collection[24] whereas a third UCAMM identified in a collection from Dome Fuji had a D/H ratio compatible with terrestrial values[25]. UCAMMs are key samples for giving a better understanding of the nature and isotopic characteristics of OM on small icy bodies from external regions of the Solar System and for comparing their organic components to those reported in samples from inner Solar System objects.

In this work, we report hydrogen, carbon and nitrogen isotopic compositions of four UCAMMs from the Concordia collection[28]: DC06-05-94 (DC06-94), DC06-07-18 (DC06-18), DC16-14-309 (DC16-309) and DC06-04-43 (DC06-43) (Fig. 1). They were analysed by nanoscale secondary-ion mass spectrometry (NanoSIMS) at the Institut Curie (France), the Muséum National d'Histoire Naturelle (France) and the Carnegie Institution for Science (United States).

Results

Isotopic compositions of UCAMMs

We performed isotopic mapping of the D/H, $^{15}N/^{14}N$ and $^{13}C/^{12}C$ ratios of the four UCAMMs (Fig. 2, Extended Data Figs. 1, 2 and 3 and Extended Data Table 1) to provide an overview of the bulk spatial distribution of their compositions and to pinpoint local anomalies within the particles. Scatter plots for the four measured UCAMMS are shown in Fig. 3. The histograms along the axes show the distribution in µm² associated with each isotopic composition. The average δD, $\delta^{15}N$ and $\delta^{13}C$ values are reported in Table 1 with uncertainties indicating the spread of isotopic values within single UCAMMs (local heterogeneities). Values are reported with one standard deviation.

The DC06-94 fragment is the largest of the four UCAMMs analysed. It has a total surface area of 9,652 µm². It is characterized by a bulk $\delta D_{DC94} = 2{,}700 \pm 1{,}600$‰ and extreme D-rich zones reaching values greater than 15,000‰, which are comparable to extreme values reported previously for one UCAMM[19]. These large D/H ratios occur both in diffuse areas and discrete hotspots (Fig. 3). The distribution of $\delta^{15}N$ in DC06-94 is centred around $\delta^{15}N_{DC94} = 75 \pm 67$‰ with a range from −149 up to +547‰. We measured the carbon isotopic composition of DC06-94 in four zones with a total area of 602 µm² (Fig. 2a). The average composition was ^{13}C-depleted: $\delta^{13}C_{DC94} = -93 \pm 31$‰. A correlation between δD and $\delta^{13}C$ was observed at a 1–10 µm scale (Extended Data Fig. 4).

The area of DC06-43 analysed was 38 µm². The isotopic composition of DC06-43 has lower variations than DC06-94. It is enriched in both D and ^{15}N ($\delta D_{DC43} = 3{,}600 \pm 1{,}100$‰ and $\delta^{15}N_{DC43} = 282 \pm 67$‰) but its $^{13}C/^{12}C$ is compatible with that of standard Pee Dee belemnite ($\delta^{13}C_{DC43} = 4 \pm 19$‰).

Three fragments of DC06-18, with a total area of 753 µm², were analysed. DC06-18 has the lowest bulk δD measured in UCAMMs from the Concordia collection: $\delta D_{DC18} = 950 \pm 390$‰. It has a depleted ^{15}N composition with $\delta^{15}N$ ranging from −224‰ to −60‰, a rather smooth distribution (no hot or cold spots) and an average value of $\delta^{15}N_{DC18} = -122 \pm 34$‰. The $\delta^{13}C$ distribution of DC06-18 is also homogeneous, with an average $\delta^{13}C_{DC18} = -6 \pm 7$‰.

The area of DC16-309 analysed was the smallest studied (about 8 µm²). It displays a D-rich composition with values ranging from 4,150 to 8,730‰ (average $\delta D_{DC309} = 7{,}300 \pm 1{,}500$‰). Notably, D enrichments are associated with large ^{15}N depletions ranging from −169 to −22‰, with an average $\delta^{15}N_{DC18} = -121 \pm 56$‰. Moreover, isotopic plots of DC16-309 reveal an anticorrelation between the D/H and $^{15}N/^{14}N$ ratios, as illustrated in Fig. 3a. The OM of DC16-309 has a slightly ^{13}C-enriched bulk composition ($\delta^{13}C_{DC43} = 34 \pm 5$‰).

Discussion

Comparison with organics in chondrites and IDPs

It has been discussed whether IOM from chondrites originates from a single common OM precursor[1,31]. The diversity of bulk isotopic compositions of light elements in UCAMMs revealed in the present study indicates that this is most probably not the case for cometary OM. Despite their isotopic diversity, a key feature of all UCAMMs from the Concordia collection is their large excesses in D, with average δD ranging from 950 to 7,300‰ (Table 1 and Extended Data Fig. 4), which is at odds with the UCAMM D05IB80 from the Dome Fuji collection[25]. The isotopic compositions of H, C and N in UCAMMs exhibit similarities with those reported in organics in meteorites (organic clasts, nanoglobules and IOM) and IDPs, as shown in Fig. 4.

The bulk isotopic compositions of OM in DC06-43 exhibit a rather straightforward similarity with that reported in CR chondrites, with similar bulk δD and $\delta^{15}N$ signatures[1,2] (Fig. 4 and Extended Data Fig. 5) but higher than bulk values reported for IOM from most other chondrites. Average values from this OM do not exceed $\delta^{15}N \approx 400$‰ and $\delta D \approx 3{,}600$‰. The recent identification of a carbon-rich clast within

https://doi.org/10.1038/s41550-024-02364-y

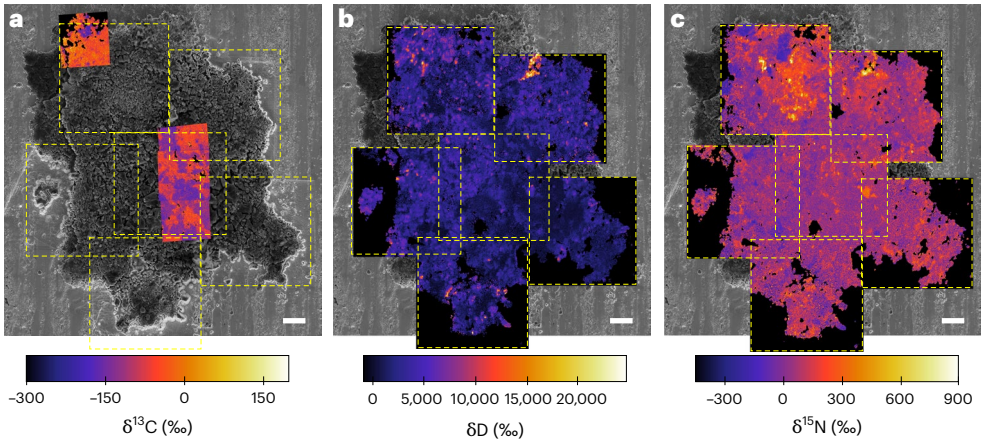

Fig. 2 | Fragment of UCAMM DC06-94 crushed on gold and analysed by NanoSIMS. a, Secondary electron image of the fragment, with four superimposed $\delta^{13}C$ maps. **b**,**c**, δD (**b**) and $\delta^{15}N$ (**c**) isotopic maps of the whole DC06-94 fragment from the combination of six 50-µm-sized raster maps. Scale bars, 10 µm.

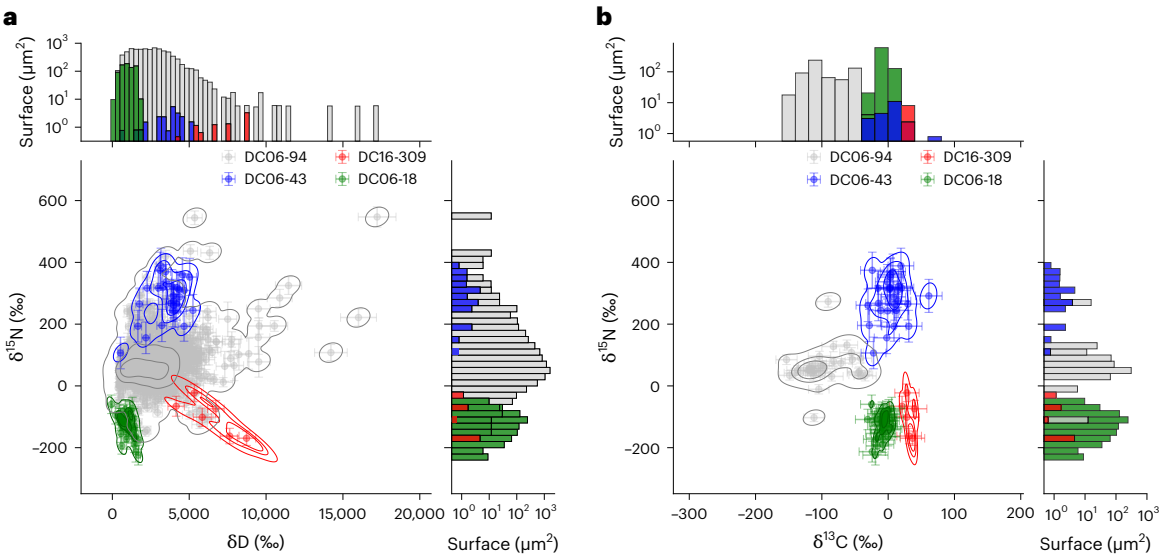

Fig. 3 | Isotopic compositions of UCAMMs DC06-94 (grey), DC06-43 (blue), DC06-18 (green) and DC16-309 (red). Side histograms indicate the area analysed in µm² (log scale). **a**, $\delta^{15}N$ versus δD compositions. **b**, $\delta^{15}N$ versus $\delta^{13}C$ compositions. Data points are the mean isotopic ratios measured in individual ROIs ± one standard deviation ('Data reduction' in Methods and Supplementary Table 1). The solid lines are the isodensity contours of the density functions at 5% (threshold), 33% and 66%.

the CR2 chondrite LaPaz Icefield 02342 (ref. 4) indicates that the OM in the CR parent body is most probably closely linked to a cometary reservoir. This cometary heritage has also been suggested due to the similarities of CR chondrites' IOM with CHON grains collected from comet Halley by the Vega mission[1,32] and pristine IDPs. Several IDPs have average H, C and N isotopic values and structures comparable to those observed in DC06-43 (Fig. 4 and Extended Data Figs. 5 and 6), IOM from CR chondrites and grains from comet 81P/Wild 2 (ref. 17), all of which have local extreme D and ^{15}N enrichments[10,11]. It has been proposed that IDPs with such characteristics may originate from the Jupiter-family comet 26P/Grigg–Skjellerup (ref. 15). Based on their bulk isotopic compositions and their heterogeneous distributions, the organics in DC06-43 probably originated from a cometary object, possibly a Jupiter-family comet, like those considered for numerous IDPs[12]. Such an origin is also supported by elemental N/C ratios reported for DC06-43 (0.04 ± 0.03)[27] and grains from comet 67P/Churyumov–Gerasimenko (0.035 ± 0.011)[33]. OM in these objects is characterized by a composition globally enriched in both D and ^{15}N, with an average $\delta^{15}N$ ranging from 150 to 400‰ and δD from 2,000 to 5,000‰. Interestingly, that OM from CR chondrites and DC06-43 share analogous H, C and N isotopic compositions and N/C ratio (0.032–0.044) indicates that their respective parent bodies may have accreted a common precursor.

The isotopic compositions of both H and N in DC06-94, in association with the occurrence of numerous D and ^{15}N hotspots (with $\delta D \simeq 15{,}000$‰ and $\delta^{15}N \simeq 600$‰), are consistent with data reported for CI and CR chondrites. However, this UCAMM exhibits an unusual ^{13}C-poor isotopic composition. Although the occurrence of micrometre-sized areas with comparable ^{13}C depletion have been reported for CR, CI, CO and CM chondrites (Fig. 4), such carbon phases remain rare and the C isotopes in DC06-94 stand apart from most reported extraterrestrial OM. Noticeably, the DC06-94 N/C ratio ($0.05^{+0.05}_{-0.02}$)[26] is comparable to that observed in DC06-43 and CR chondrites.

In contrast, the isotopic compositions of UCAMMs DC06-18 and DC16-309 are clearly distinct from those discussed above. They exhibit ^{15}N-depleted bulk signatures, with $\delta^{15}N \simeq -120$‰ and with no D, ^{15}N or ^{13}C hotspots (Fig. 3 and Extended Data Fig. 5). Such bulk signatures are not commonly observed, neither in IOM from meteorites nor in IDPs with the exception of CP IDPs Eliot[11], Polo[13], Hawkins[13] and Porky[10],

https://doi.org/10.1038/s41550-024-02364-y

Table 1 | Average δD, $\delta^{15}N$ and $\delta^{13}C$ values measured for the four UCAMMs and corresponding surface areas analysed per particle

UCAMM		δD (‰)	$\delta^{15}N$ (‰)	$\delta^{13}C$ (‰)	Area analysed (μm²)
DC16-309	Bulk	7,300±1,500	−121±56	34±5	8
	Q_1–Q_3	5,460 to 7,404	−147 to −68	28 to 35	
	Min–Max	4,150 to 8,730	−169 to −22	21 to 39	
DC06-43	Bulk	3,600±1,100	282±67	4±19	38
	Q_1–Q_3	3,150 to 4,250	244 to 319	−4 to 14	
	Min–Max	530 to 5,240	107 to 389	−31 to 61	
DC06-18	Bulk	950±390	−122±34	−6±7	753
	Q_1–Q_3	640 to 1,290	−152 to −101	−11 to −2	
	Min–Max	−59 to 1,730	−224 to −60	−31 to 7	
DC06-94	Bulk	2,700±1,600	75±67	*−93±31*[a]	9,652 *(602*[a]*)*
	Q_1–Q_3	1,570 to 3,470	38 to 103	*−115 to −71*[a]	
	Min–Max	370 to 17,200	−149 to 547	*−153 to −35*[a]	

The uncertainties are derived from one standard deviation of the distributions of isotopic values. They represent the range of the isotopic values measured in different ROIs, that is, the local heterogeneities within UCAMMs. Q_1 and Q_3 are the first and third quartiles of the distributions of isotopic values. Min and Max are the extreme values measured for the UCAMMs. [a]The $\delta^{13}C$ values of UCAMM DC06-94 were measured for the subset of areas indicated in Fig. 2a. Numerical values for this subset are indicated in italics.

which have bulk ^{15}N compositions of $\delta^{15}N = -108 \pm 9‰$, $-167 \pm 9‰$, $-190 \pm 27‰$ and $-93 \pm 4‰$, respectively. The bulk ^{13}C compositions of Eliot ($\delta^{13}C = 14 \pm 18‰$), Polo ($12 \pm 8‰$) and Hawkins ($21 \pm 13‰$) are also consistent with the values reported for DC06-18 and DC06-309. Porky is more ^{13}C-depleted ($\delta^{13}C = -53 \pm 2‰$). Unlike the other IDPs studied by Floss et al.[11] and Davidson et al.[13], Eliot, Polo and Hawkins exhibit a smooth platy OM component with very few or no ^{15}N-rich hotspots relative to their bulk composition. Similarly, DC06-18 and DC16-309 do not present the anomalous ^{15}N hotspots observed in DC06-94 (Fig. 2), although one should keep in mind that the area analysed of DC06-94 is much larger than that of DC06-18 and DC16-309 (Extended Data Fig. 7). Notably, N/C elemental ratios measured in a fragment of DC06-18 reached 0.17 ± 0.04 (ref. 27), about four times above that measured in DC06-94 and DC06-43 and higher than in most interplanetary OM. Yet, it remains comparable to values reported for carbonaceous grains from the comet 81P/Wild 2 (ref. 34).

Similar ^{15}N depletions have been reported for rare C-rich grains and nanoglobules in Maribo[8] (CM), DOM-08006 (ref. 6) (CO) and Orgueil[35] (CI) as well as several CR chondrites[3,5,7,9] and IDPs[14] (Fig. 4). Vollmer et al.[8] associated those grains with primordial organics that have not been altered based on their C and N functional chemistry signatures (highly aromatic carbon, absence of carboxylic functional groups and presence of imine or nitrile functional groups), possibly inherited from the interstellar medium. Such an origin is consistent with an outer Solar System origin for UCAMMs. Interestingly, the anomalous C-grains in DOM-08006 have ^{13}C and ^{15}N signatures analogous to those of the four UCAMMs, reflecting that the different isotopic signatures reported in distinct UCAMMs can coexist at small scales within meteorites and implying that they may reflect reservoirs that predate the incorporation of organics in extraterrestrial objects. Recent studies of carbon-rich grains in Ryugu particles showed that both ^{15}N-rich and -poor OM grains are present in asteroids[18] (Extended Data Fig. 8), confirming that, even if less abundant, the ^{15}N-poor OM observed in UCAMMs is present at different heliocentric distances.

Isotopic fractionation in the early Solar System

The isotopic compositions of nitrogen measured in the atmosphere of Jupiter ($\delta^{15}N = -375 \pm 80‰$)[36], in samples of the solar wind returned by the Genesis spacecraft ($\delta^{15}N = -383 \pm 8‰$)[37] and in high-temperature solar-nebula condensates in meteorites ($\delta^{15}N = -359 \pm 5‰$)[38] all indicate that the main nitrogen reservoir in the protosolar disk, N_2, was ^{15}N-depleted. This primordial component is not commonly observed in interplanetary materials, for which OM and IOM usually exhibit higher $^{15}N/^{14}N$. The low ^{15}N component identified in DC16-309 and DC06-18 in this study may, thus, derive from the preservation of some of this main initial gas reservoir of N_2. DC06-94 and DC06-43, on the other hand, like most IDPs and CR chondrites, most probably derived from another reservoir that was globally enriched in ^{15}N compared to the main nitrogen reservoir. The bulk $^{13}C/^{12}C$ ratio of the early Solar System remains a matter of debate[39–41], although measurements of the solar wind implanted in the lunar regolith[39] and direct measurements of the solar wind with the solar wind ion composition spectrometer[40] suggest a ^{13}C-depleted reservoir, with a value below $\delta^{13}C \approx -90‰$. Such a value is lower than bulk values reported in most chondritic IOM and IDPs but is comparable to the ^{13}C-poor OM observed in one UCAMM from this study (DC06-94). Still, the measurements made by the solar wind ion composition spectrometer have large uncertainties, and those values are substantially lower than that derived from CO emission lines in the solar photosphere ($\delta^{13}C = -48 \pm 7‰$)[41]. Remote and in situ sensing of comets has revealed that, although most of their C-bearing molecules (including CO and CO_2) have $^{13}C/^{12}C$ ratios like those reported for carbonaceous chondrite and the Earth[21], their HCN is ^{13}C-poor, with values ranging from $\delta^{13}C = -179 \pm 105‰$ to $\delta^{13}C = -215 \pm 179‰$ (refs. 23,42). Cometary CN is characterized by higher $^{13}C/^{12}C$ ratios[22], suggesting that the originating reservoirs for HCN and CN were isotopically distinct. The lack of correspondence between the solar N and C isotopic compositions and the isotopic signature of interplanetary OM suggest that, as for hydrogen ('Isotopic fractionation of hydrogen' in Methods)[19], the isotopic fractionation of N- and C-bearing species occurred before the formation of the OM observed in these objects.

Several astrochemistry models[19,20] that describe the evolution of species in the protoplanetary disk under the effects of both physical and chemical processes can predict the isotopic fractionation of light elements in the early Solar System. Aikawa et al.[19] studied hydrogen isotopic fractionation and showed that extreme D enrichments are expected in different species (for example HCOOH, CH_3CN and NH_3) within 10^5 years of the formation of the protostellar core at heliocentric distances above $R \approx 20$ au. Visser et al.[20] highlighted that the complex chemistry of C- and N-bearing molecules in the protoplanetary disk can lead to strong isotopic fractionation, depending on the specific molecular species and on both the radial and azimuthal positions in the disk. The latter authors predicted complex zonation patterns in the disk during the isotopic fractionation of molecular species such as N_2, HCN, NH_3, CN and CO. Such patterns are schematized for arbitrary chemical species by the colour scale in the top panel of Fig. 5. According to their model, the isotope-selective UV photodissociation of N_2 is the main process affecting N isotopic fractionation in the protoplanetary disk. It leads to ^{15}N depletion (relative to the primordial signature) in both N_2 and NH_3 reservoirs and enrichment of cyanides at the disk surface while having a limited impact at the midplane[20]. Although the isotopic fractionation of carbon in the disk is also expected to be affected by isotope-selective photodissociation of CO, low-temperature exchange reactions initiated below 30 K in the midplane can counterbalance this fractionation[20]. The resulting C isotopic compositions in the different gaseous species highly depends on the balance of these two processes. At the scale of the disk, based on the model, the CO reservoir tends to be ^{13}C-rich compared to cyanides (echoing remote-sensing data for comets), the latter being a possible carrier of the ^{13}C-poor composition in DC06-94. However, a ^{13}C-rich CO reservoir is at odds with what is expected from the solar and Jovian $^{13}C/^{12}C$ (ref. 41).

Formation of isotopically anomalous N-rich OM

The origin of UCAMMs is highly constrained by their exceptionally high concentration of OM and depletion in minerals[24,26]. UCAMMs usually

https://doi.org/10.1038/s41550-024-02364-y

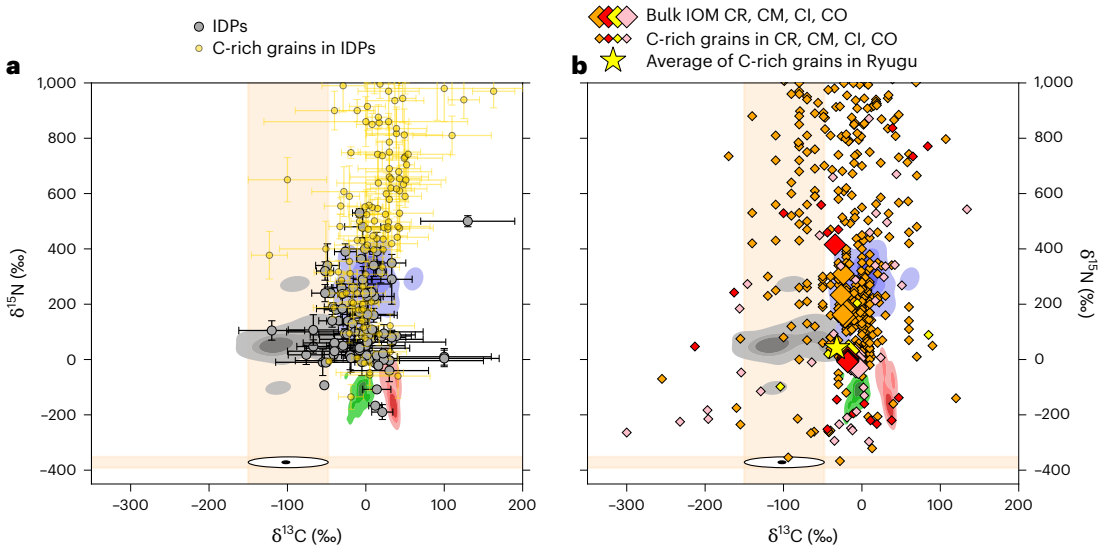

Fig. 4 | Comparison of the C and N isotopic composition of the four analysed UCAMMs with literature data. a,**b**, DC06-94, DC06-43, DC06-18 and DC16-309 are shown with grey, blue, green and red shading. Literature data for IDPs (**a**) and carbonaceous matter from meteorites (**b**) are superimposed. Bulk IDPs[10–15] and hotspots in IDPs[11–14] are indicated in **a** as dark grey dots and yellow dots with one standard deviation error bars. In **b**, bulk IOM data are indicated as large diamonds for CR (orange), CM (red), CI (yellow) and CO (pink) chondrites[1]. Carbonaceous grains in CR, CM, CI and CO chondrites[3,5–9] are shown as small diamonds with the same colour code. The average composition of grains from the carbonaceous asteroid Ryugu[18], which were returned by the Japan Aerospace Exploration Agency's return sample mission Hayabusa2, is reported as a yellow star. The shaded area and the ellipse represent the range of variation of the solar $\delta^{15}N$ and $\delta^{13}C$ values. Extended Data Fig. 6 displays the same data over a larger range including higher $\delta^{15}N$ values in hotspots reported in IDPs and chondrites.

exhibit extreme C/Si ratios (≥10), higher than the interstellar value[27]. Thus, their formation cannot be explained by the direct incorporation of an interstellar or early protoplanetary disk carbonaceous heritage but requires a concentration process that must have taken place within the Solar System itself. Moreover, the large N/C ratios of UCAMMs indicate that the synthesis of such peculiar OM must have occurred in a nitrogen-rich environment[25–27].

These observations point towards a formation in the cold regions of the Solar System, where small bodies (cometary-sized objects) can accrete N- and C-rich volatile ice mantles[43,44]. According to models of fractionation in the disk[20], N- and C-bearing volatile species in the outer Solar System can be highly fractionated, leading to the formation of isotopically fractionated ice mantles (Fig. 5, steps 1 and 2). In such regions, the icy surfaces of small bodies endure irradiation by Galactic cosmic rays, which trigger chemical reactions that lead to the production of macromolecular IOM precursors[45] (Fig. 5, step 2). For the most remote objects, this irradiation is more intense due to the suppression of the Sun's magnetic field[46]. Under the effect of moderate heating episodes (for example, the insolation variation caused by seasonal and astrophysical cycles[47]), the volatile ice-mantle species sublimate (totally or partially) and the irradiation-induced macromolecular precursors, due to their refractory nature, tend to concentrate to form an organic crust (Fig. 5, step 3). Importantly, within such a process, the resulting organics are expected to have an isotopic signature deriving from that of their ice precursors, as the ion irradiation induces the recombination of molecules in the ice, leading to the transfer of the isotopic composition of the ice to the newly formed organic precursors[48]. Because the processing of the ice occurs at the very surface of the parent body, the thickness of the N-rich ice mantle prevents substantial incorporation within the synthesized OM of minerals that remain locked deeper below the volatile surface ice layers.

Laboratory experiments[45,48] of ion irradiation of ice films at 10 K have demonstrated that such a process is efficient in synthesizing a N-rich OM when starting from N-rich ices, characteristic of the surface of trans-Neptunian objects[44] (N_2 and NH_3 ices). Recent experiments have also showed that, although irradiation itself does not induce substantial isotopic fractionation in the synthesized OM, large isotopic heterogeneities can be imprinted in the OM by irradiating isotopically layered ice films[48,49]. In such experiments, the bulk isotopic signature of the irradiation-induced OM reflects that of the bulk ice whereas micrometre-scale heterogeneities are related to the pre-irradiation fine-scale mixing of ices with distinct isotopic signatures.

The diversity of the bulk isotopic signatures of UCAMMs suggests that they do not originate from a unique reservoir or a unique average ice composition. The N-rich and ^{15}N-depleted OM of DC06-18 and DC16-309 can be obtained through the irradiation of an ice mantle with a substantial contribution of ^{15}N-poor N_2. Such a contribution from the primordial N_2 reservoir points toward the outer regions of the Solar System, where the temperature is low enough for small bodies to retain hypervolatiles at their surface[44] (Fig. 5b). The parent body of DC16-309 and DC06-18 could, thus, be a remote object, possibly an object from the outer Kuiper belt or an Oort cloud comet. The OM of DC06-94 and DC06-43 could have originated from the irradiation of the surface mantle of a parent body consisting of a different mixture of ices. Its ^{15}N-rich signature suggests a small contribution of the primordial N_2 reservoir, which may indicate a warmer environment (Fig. 5a), possibly in the Kuiper belt, where volatile species such as cyanides condense and for which models predict ^{15}N enrichment[20]. When entering the inner Solar System, these icy bodies exhibit enhanced surface activity leading to the release of fragments of their organic crusts, which feeds the interplanetary medium with organic-rich particles such as UCAMMs (Fig. 5, step 4). Particles from the surface of Kuiper belt objects could also be released by recent collisions in this very region and subsequently drift to the inner regions, as recently proposed by Keller and Flynn[50].

The similarities between the OM from DC06-43 and that of CR chondrites suggest that they may have been synthesized from a similar precursor. However, IOM in CR chondrites formed before the formation of the CR parent body, and this seems to be incompatible with the irradiation time required to process the surface ice mantle (~10^7 years) of the parent body of DC06-94 and DC06-43. Due to the possible remote location of the synthesis of the OM in DC16-309 and DC06-18, similar OM in other interplanetary objects could be less frequent, explaining

https://doi.org/10.1038/s41550-024-02364-y

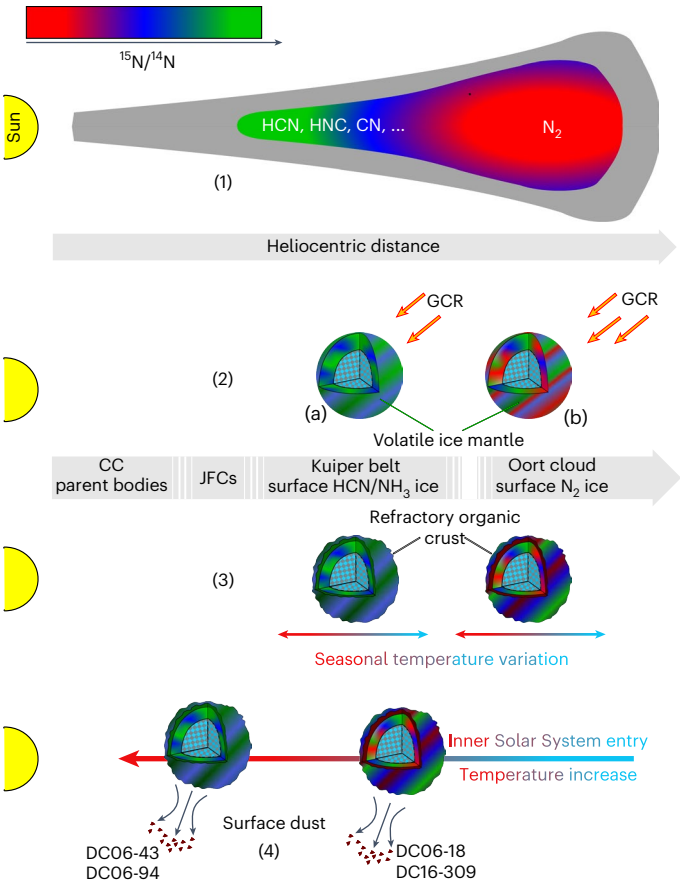

Fig. 5 | Sketch of the formation of UCAMM N-rich OM. (1) N-bearing species are isotopically fractionated in the protoplanetary disk, with the fractionation depending on the chemical species. Primordial N_2 is ^{15}N-poor compared to other species such as HCN, HNC, CN, as represented with the colour scale. (2) The parent bodies of UCAMMs accrete a N-rich isotopically heterogeneous ice mantle. Although most of the small bodies retain less volatile molecules (**a**), only the coldest are able to retain ^{15}N-poor N_2 ice at their surface (**b**). The ice mantles are processed by Galactic cosmic rays (GCRs), leading to the formation of new molecules that are precursors of the UCAMM OM. (3) Heating episodes caused by eccentric orbits (surface heating as the body approaches the Sun marked by the blue and red arrows) lead to the sublimation of the ice mantles and the concentration of the precursors to form a refractory, N-rich, isotopically heterogeneous, macromolecular, organic crust. The bulk isotopic composition and the local heterogeneities of such an organic crust derive from the past history of its initial ice-mantle freeze-out at various heliocentric distances. (4) When entering the inner Solar System, the temperature increase (blue and red arrow) triggers surface activity, leading to the ejection of surface dust and giving rise to UCAMMs. CC, carbonaceous chondrite; JFCs, Jupiter-family comets.

why this OM is, so far, rather specific to UCAMMs. Given the technical challenges of visiting trans-Neptunian regions with sample return space missions, UCAMMs represent a unique way to shed light on the elemental and isotopic compositions of the processed surface ice layers of the outermost objects of the Solar System.

Methods

Collecting the Antarctic micrometeorites

The UCAMMs studied in this work are from the Concordia collection[28,51]. These micrometeorites were extracted from volumes of clean snow excavated from the subsurface (3.3–9 m deep) of the central Antarctic plateau around the Dome C station (75° 06' S, 123° 20' E). The snow was slowly melted in a dedicated stainless steel melter and sieved with 20 to 30 µm mesh filters. The filters were processed in a dedicated clean room (ISO 7) under a clean hood at IJCLab (France, formerly the Centre for Nuclear Spectrometry and Mass Spectrometry). Candidate UCAMMs were hand-picked and fragmented. A fragment of each was subsequently deposited onto carbon tape (Fig. 1) and examined by scanning electron microscopy and energy-dispersive X-ray spectrometry for identification and classification. UCAMMs, in addition to presenting a chondritic elemental pattern, are characterized by large amounts of carbon in their energy-dispersive X-ray spectra (>50 vol%)[27]. When identified as being an UCAMM, fragments of the particle were prepared for different analytical techniques, including NanoSIMS. NanoSIMS and other techniques were not performed on the fragments fixed to the carbon tape. Complementary fragments of UCAMMs presented in this work were previously analysed with complementary non-destructive techniques including infrared and Raman spectroscopy[26,27,52], scanning transmission electron microscopy[30], scanning transmission X-ray microscopy of X-ray absorption near edge structures and the atomic force microscopy infrared technique (nanometre-scale infrared)[53].

Sample analyses

The surface of DC06-94 presented in this work resulted from the crushing of a large fragment onto gold foil. Carbon isotopic data ($^{12}C^-$ and $^{13}C^-$ ions) were acquired with the NanoSIMS 50 instrument at the Muséum National d'Histoire Naturelle (Paris, France) with a 1 pA Cs^+ ion probe. Nitrogen and hydrogen isotopic data ($^{12}C^{14}N^-$, $^{12}C^{15}N^-$, $^{12}C_2H^-$ and $^{12}C_2D^-$ ions) were acquired with the NanoSIMS 50 instrument at Institut Curie/Laboratoire des Multimatériaux et Interfaces (IC/LMI, France) with an 8–12 pA Cs^+ ion probe. The instrumental mass fractionations were controlled using characterized standards: a type III kerogen and the natural anthracite DonH8 (ref. 54). Three fragments of DC06-18 were crushed onto gold foil whereas a DC06-43 fragment was pressed onto a diamond window. The fragment of UCAMM DC16-309 was embedded in sulfur and ultramicrotomed. The resulting thin slice was deposited onto a diamond window and gently annealed at 50 °C to remove the remaining sulfur. This thin slice was also analysed by the atomic force microscopy infrared technique[53]. All samples were coated with a 20-nm-thick gold layer before the NanoSIMS analysis to ensure the conductivity of the sample was adequate. DC06-18, DC06-43 and DC16-309 were analysed with the NanoSIMS 50 L instrument at the Carnegie Earth and Planets Laboratory (Washington, DC). The hydrogen, carbon and nitrogen isotopic compositions were derived from H^-, D^-, $^{12}C_2^-$, $^{12}C^{13}C^-$, $^{12}C^{14}N^-$ and $^{12}C^{15}N^-$ ions using a 10 pA Cs^+ ion probe. We used an in-house standard $C_{30}H_{50}O$, IOM from the CR chondrite Queen Alexandra Range 99177, and SiC and Si_3N_4 standards to control the instrumental mass fractionations. The dimensions and spatial resolutions of the NanoSIMS acquisitions for the four UCAMMs are given in Extended Data Table 1.

Data reduction

Raw sequences of ion images[55] were extracted using the OpenMIMS plug-in (funded by the National Institutes of Health and the National Institute of Biomedical Imaging and Bioengineering as a National Resource) of the ImageJ software[56]. Ion images in a sequence were aligned using a dedicated TomoJ plug-in[57] of the ImageJ software. Aligned sequences of images were subsequently summed, and a mask was defined above a minimum threshold of the emission of the main isotope to avoid spurious effects caused by low counting statistics. Advanced treatments were performed with dedicated routines written in the Python programming language (Python Software Foundation, https://www.python.org/). Dead-time corrections were applied. The impact of quasi-simultaneous arrivals[58] was investigated for $^{12}C_2^-$ and $^{12}C^{14}N^-$ ions by assuming a constant correction coefficient $\beta = 1/2$, which resulted in average fractionations of about 5‰. Although the value of β differs with the nature of the ions, its empirical determination is probably impacted by the nature of the sample[58], leading to potential under- or overcorrections. Considering the limited magnitude of the corrections for quasi-simultaneous arrivals on the results and to avoid

spurious correction effects, the results presented in this study were not corrected for quasi-simultaneous arrivals. We derived the local isotopic composition of the UCAMMs by mapping the ion images with a hexagonal mesh to fully pave the two-dimensional maps (for DC06-94 and DC06-43) or with local regions of interest (ROIs, for DC16-309 and DC06-18) when the orientations of the H, C and N acquisitions differed. For two isotopes ^{A}X and ^{A+1}X of element X with mass numbers A and A+1, the ion emissions of each hexagonal cell (respectively, ROI), N_i for ^{A}X and $\tilde{N}_i$ for ^{A+1}X, are equal to the sum of the pixels of the cell (respectively, ROI), $n(^{A}X)$ and $n(^{A+1}X)$. The corresponding isotopic ratio (R_i) is given by the ratio of the ion emissions of the two isotopes in the cell (respectively, ROI). Errors on the ion emission (σ_{R_i}) are given by the Poisson statistics:

$$R_i = \frac{\tilde{N}_i}{N_i} = \frac{\sum_{\text{pixels in i}} n(^{A+1}X)}{\sum_{\text{pixels in i}} n(^{A}X)},$$

$$\sigma_{R_i} = \left(\frac{\sqrt{\tilde{N}_i}}{\tilde{N}_i} + \frac{\sqrt{N_i}}{N_i} \right) \times \frac{\tilde{N}_i}{N_i}.$$

We treated the standard measurements according to the same procedure. We derived the reproducibility of the isotopic values of standards from the dispersion of the isotopic ratios measured in the cells of the hexagonal mesh $\sigma_{R_{std}}$ (one standard deviation). Thus, the correction factor for the instrumental mass fractionations is given by:

$$\alpha = \frac{\langle R_{std,i} \rangle}{R_{cal}} \pm \frac{\sigma_{R_{std}}}{R_{cal}},$$

where R_{cal} is the calibrated value of the standard.

The errors are given by the quadratic sum of the reproducibility of the standard values and the statistical errors on the counting statistics. Ion counts, isotopic ratios and associated errors measured in ROIs are provided in Supplementary Table 1.

Isotopic fractionation of hydrogen

Although the D/H ratio of the main H_2 reservoir of the protosolar nebula is estimated to be[59] D/H = (2.1 ± 0.5) × 10^{-5}, most of the H-bearing molecules in Solar System objects exhibit D/H ratios more than an order of magnitude larger[60]. D/H measurements by remote and in situ sensing in water molecules in comets show moderate variations ranging from δD ≃ −240‰ to 2,200‰ (ref. 21) with no clear correlations between the magnitude of the D enrichment and the comet type. HCN detected in the coma of the comet Hale–Bopp[61] and linear alkanes measured in situ in comet 67P/Churyumov–Gerasimenko[21] have higher δD ≃ 12,200–14,500‰. Higher δD have been reported for NH_3, H_2CO and CH_3OH for these two comets. However, refractory organics measured by the COSIMA instrument onboard the Rosetta spacecraft exhibited lower δD = (9,100 ± 3,500‰)[62], comparable to D enrichments observed in UCAMMs (DC16-309 and in ref. 24). Compared to the main primordial carrier of H in the interstellar medium (H_2), large D enrichments are observed in more complex (secondary) molecules. These enrichments, which were caused by ion–molecule reactions[63], are predicted to happen most probably in the interstellar medium or at the nebular stage[60], leading to an increasing D/H gradient from the inner to the outer Solar System[19]. According to models of disk formation[19], D/H ratios in species such as CH_4, HCOOH, CH_3COOH and NH_3 can be up to four orders of magnitude higher than that of primordial H_2. As most of the complex H-bearing molecules are expected to be D-rich, associating a H isotopic signature to a specific reservoir is not straightforward. The relative homogeneity of the D/H measured in H-bearing species (excluding water) in comets[21] also tends to indicate the difficulty of linking a D/H to a specific volatile parent reservoir.

Data availability

The data presented in the paper are provided in Supplementary Table 1 and are available via Zenodo at https://doi.org/10.5281/zenodo.12626220 (ref. 55).

References

1. Alexander, C. M. O'D., Fogel, M., Yabuta, H. & Cody, G. D. The origin and evolution of chondrites recorded in the elemental and isotopic compositions of their macromolecular organic matter. *Geochim. Cosmochim. Acta* **71**, 4380–4403 (2007).
2. Busemann, H. et al. Interstellar chemistry recorded in organic matter from primitive meteorites. *Science* **312**, 727–730 (2006).
3. De Gregorio, B. T. et al. Isotopic and chemical variation of organic nanoglobules in primitive meteorites. *Meteorit. Planet. Sci.* **48**, 904–928 (2013).
4. Nittler, L. R. et al. A cometary building block in a primitive asteroidal meteorite. *Nat. Astron.* **3**, 659–666 (2019).
5. Floss, C. & Stadermann, F. J. High abundances of circumstellar and interstellar C-anomalous phases in the primitive CR3 chondrites QUE 99177 and MET 00426. *Astrophys. J.* **697**, 1242 (2009).
6. Nittler, L. R. et al. High abundances of presolar grains and ^{15}N-rich organic matter in CO3.0 chondrite Dominion Range 08006. *Geochim. Cosmochim. Acta* **226**, 107–131 (2018).
7. Vollmer, C. et al. Isotopic compositions, nitrogen functional chemistry, and low-loss electron spectroscopy of complex organic aggregates at the nanometer scale in the carbonaceous chondrite Renazzo. *Meteorit. Planet. Sci.* **55**, 1293–1319 (2020).
8. Vollmer, C. et al. A primordial ^{15}N-depleted organic component detected within the carbonaceous chondrite Maribo. *Sci. Rep.* **10**, 20251 (2020).
9. Floss, C., Le Guillou, C. & Brearley, A. Coordinated NanoSIMS and FIB-TEM analyses of organic matter and associated matrix materials in CR3 chondrites. *Geochim. Cosmochim. Acta* **139**, 1–25 (2014).
10. Messenger, S. Identification of molecular-cloud material in interplanetary dust particles. *Nature* **404**, 968–971 (2000).
11. Floss, C. et al. Identification of isotopically primitive interplanetary dust particles: a NanoSIMS isotopic imaging study. *Geochim. Cosmochim. Acta* **70**, 2371–2399 (2006).
12. Floss, C., Stadermann, F. J., Mertz, A. F. & Bernatowicz, T. J. A NanoSIMS and Auger nanoprobe investigation of an isotopically primitive interplanetary dust particle from the 55P/Tempel-Tuttle targeted stratospheric dust collector. *Meteorit. Planet. Sci.* **45**, 1889–1905 (2010).
13. Davidson, J., Busemann, H. & Franchi, I. A. A NanoSIMS and Raman spectroscopic comparison of interplanetary dust particles from comet Grigg–Skjellerup and non-Grigg Skjellerup collections. *Meteorit. Planet. Sci.* **47**, 1748–1771 (2012).
14. Matrajt, G., Messenger, S., Brownlee, D. & Joswiak, D. Diverse forms of primordial organic matter identified in interplanetary dust particles. *Meteorit. Planet. Sci.* **47**, 525–549 (2012).
15. Busemann, H. et al. Ultra-primitive interplanetary dust particles from the comet 26P/Grigg/Skjellerup dust stream collection. *Earth Planet. Sci. Lett.* **288**, 44–57 (2009).
16. Aléon, J., Engrand, C., Robert, F. & Chaussidon, M. Clues on the origin of interplanetary dust particles from the isotopic study of their hydrogen-bearing phases. *Geochim. Cosmochim. Acta* **65**, 4399–4412 (2001).
17. McKeegan, K. D. et al. Isotopic compositions of cometary matter returned by Stardust. *Science* **314**, 1724–1728 (2006).
18. Yabuta, H. et al. Macromolecular organic matter in samples of the asteroid (162173) Ryugu. *Science* **379**, eabn9057 (2023).

19. Aikawa, Y., Wakelam, V., Hersant, F., Garrod, R. T. & Herbst, E. From prestellar to protostellar cores. II. Time dependence and deuterium fractionation. *Astrophys. J.* **760**, 55 (2012).
20. Visser, R. et al. Nitrogen isotope fractionation in protoplanetary disks. *Astron. Astrophys.* **615**, A75 (2018).
21. Müller, D. R. et al. High D/H ratios in water and alkanes in comet 67P/Churyumov-Gerasimenko measured with Rosetta/ROSINA DFMS. *Astron. Astrophys.* **662**, A69 (2022).
22. Manfroid, J. et al. The CN isotopic ratios in comets. *Astron. Astrophys.* **503**, 613–624 (2009).
23. Bockelée-Morvan, D. et al. Large excess of heavy nitrogen in both hydrogen cyanide and cyanogen from comet 17P/Holmes. *Astrophys. J.* **679**, L49–L52 (2008).
24. Duprat, J. et al. Extreme deuterium excesses in ultracarbonaceous micrometeorites from central Antarctic snow. *Science* **328**, 742–745 (2010).
25. Yabuta, H. et al. Formation of an ultracarbonaceous Antarctic micrometeorite through minimal aqueous alteration in a small porous icy body. *Geochim. Cosmochim. Acta* **214**, 172–190 (2017).
26. Dartois, E. et al. Ultracarbonaceous Antarctic micrometeorites, probing the Solar System beyond the nitrogen snow-line. *Icarus* **224**, 243–252 (2013).
27. Dartois, E. et al. Dome C ultracarbonaceous Antarctic micrometeorites. Infrared and Raman fingerprints. *Astron. Astrophys.* **609**, 27 (2018).
28. Duprat, J. et al. Micrometeorites from central Antarctic snow: the CONCORDIA collection. *Adv. Space Res.* **39**, 605–611 (2007).
29. Yada, T. et al. The global accretion rate of extraterrestrial materials in the last glacial period estimated from the abundance of micrometeorites in Antarctic glacier ice. *Earth Planets Space* **56**, 67–79 (2004).
30. Dobrică, E., Engrand, C., Leroux, H., Rouzaud, J.-N. & Duprat, J. Transmission electron microscopy of CONCORDIA ultra-carbonaceous Antarctic micrometeorites (UCAMMs): mineralogical properties. *Geochim. Cosmochim. Acta* **76**, 68–82 (2012).
31. Remusat, L., Guan, Y., Wang, Y. & Eiler, J. M. Accretion and preservation of D-rich organic particles in carbonaceous chondrites: evidence for important transport in the early Solar System nebula. *Astrophys. J.* **713**, 1048–1058 (2010).
32. Krueger, F. R. & Kissel, J. The organic component in dust from comet Halley as measured by the PUMA mass spectrometer on board Vega 1. *Nature* **326**, 755–760 (1987).
33. Fray, N. et al. Nitrogen-to-carbon atomic ratio measured by COSIMA in the particles of comet 67P/Churyumov–Gerasimenko. *Mon. Not. R. Astron. Soc.* **469**, S506–S516 (2017).
34. Cody, G. D. et al. Quantitative organic and light-element analysis of comet 81P/Wild 2 particles using C-, N-, and O-μ-XANES. *Meteorit. Planet. Sci.* **43**, 353–365 (2008).
35. Remusat, L., Bonnet, J.-Y., Bernard, S., Buch, A. & Quirico, E. Molecular and isotopic behavior of insoluble organic matter of the Orgueil meteorite upon heating. *Geochim. Cosmochim. Acta* **263**, 235–247 (2019).
36. Owen, T., Mahaffy, P. R., Niemann, H. B., Atreya, S. & Wong, M. Protosolar nitrogen. *Astrophys. J.* **553**, L77–L79 (2001).
37. Marty, B., Chaussidon, M., Wiens, R. C., Jurewicz, A. J. G. & Burnett, D. S. A ^{15}N-poor isotopic composition for the Solar System as shown by Genesis solar wind samples. *Science* **332**, 1533 (2011).
38. Meibom, A. et al. Nitrogen and carbon isotopic composition of the Sun inferred from a high-temperature solar nebular condensate. *Astrophys. J.* **656**, L33–L36 (2007).
39. Hashizume, K., Chaussidon, M., Marty, B. & Terada, K. Protosolar carbon isotopic composition: implications for the origin of meteoritic organics. *Astrophys. J.* **600**, 480 (2004).
40. Wimmer-Schweingruber, R. F., Berger, L., Köten, M., Bochsler, P. & Gloeckler, G. The 13C/12C Isotopic Ratio in the Solar Wind. *Lunar Planet. Sci.* **XLV**, 1114 (2014).
41. Lyons, J. R., Gharib-Nezhad, E. & Ayres, T. R. A light carbon isotope composition for the Sun. *Nat. Commun.* **9**, 908 (2018).
42. Biver, N. et al. Isotopic ratios of H, C, N, O, and S in comets C/2012 F6 (Lemmon) and C/2014 Q2 (Lovejoy). *Astron. Astrophys.* **589**, A78 (2016).
43. Brown, M. E., Schaller, E. L. & Fraser, W. C. A hypothesis for the color diversity of the Kuiper belt. *Astrophys. J.* **739**, L60 (2011).
44. Parhi, A. & Prialnik, D. Sublimation of ices during the early evolution of Kuiper belt objects. *Mon. Not. R. Astron. Soc.* **522**, 2081–2088 (2023).
45. Augé, B. et al. Irradiation of nitrogen-rich ices by swift heavy ions. Clues for the formation of ultracarbonaceous micrometeorites. *Astron. Astrophys.* **592**, A99 (2016).
46. Cooper, J. F., Christian, E. R., Richardson, J. D. & Wang, C. Proton irradiation of Centaur, Kuiper belt, and Oort cloud objects at plasma to cosmic ray energy. *Earth Moon Planets* **92**, 261–277 (2003).
47. Grundy, W. M. et al. Color, composition, and thermal environment of Kuiper belt object (486958) Arrokoth. *Science* **367**, eaay3705 (2020).
48. Augé, B. et al. Hydrogen isotopic anomalies in extraterrestrial organic matter: role of cosmic ray irradiation and implications for UCAMMs. *Astron. Astrophys.* **627**, A122 (2019).
49. Rojas, J. et al. Isotopic Analyses of Ion Irradiation-Induced Organic Residues, Clues on the Formation of Organics from UCAMMs. *Lunar Planet. Sci.* **LI**, 1630 (2020).
50. Keller, L. P. & Flynn, G. J. Evidence for a significant Kuiper belt dust contribution to the zodiacal cloud. *Nat. Astron.* **6**, 731–735 (2022).
51. Rojas, J. et al. The micrometeorite flux at Dome C (Antarctica), monitoring the accretion of extraterrestrial dust on Earth. *Earth Planet. Sci. Lett.* **560**, 116794 (2021).
52. Dobrică, E., Engrand, C., Quirico, E., Montagnac, G. & Duprat, J. Raman characterization of carbonaceous matter in CONCORDIA Antarctic micrometeorites. *Meteorit. Planet. Sci.* **46**, 1363–1375 (2011).
53. Mathurin, J. et al. Nanometre-scale infrared chemical imaging of organic matter in ultra-carbonaceous Antarctic micrometeorites (UCAMMs). *Astron. Astrophys.* **622**, A160 (2019).
54. Bardin, N. et al. Hydrogen isotopic fractionation in secondary ion mass spectrometry using polyatomic ions. *Int. J. Mass Spectrometr.* **393**, 17–24 (2015).
55. Rojas, J. A. et al. Raw NanoSIMS data - DC06-05-94, DC06-07-18, DC06-04-43, DC16-14-309. *Zenodo* https://doi.org/10.5281/zenodo.12626220 (2024).
56. Schneider, C. A., Rasband, W. S. & Eliceiri, K. W. NIH Image to ImageJ: 25 years of image analysis. *Nat. Methods* **9**, 671–675 (2012).
57. MessaoudiI, C., Boudier, T., Sorzano, C. O. S. & Marco, S. TomoJ: tomography software for three-dimensional reconstruction in transmission electron microscopy. *BMC Bioinform.* **8**, 288 (2007).
58. Slodzian, G., Hillion, F., Stadermann, F. J. & Zinner, E. QSA influences on isotopic ratio measurements. *Appl. Surf. Sci.* **231–232**, 874–877 (2004).
59. Geiss, J. & Gloeckler, G. Abundances of deuterium and helium-3 in the protosolar cloud. *Space Sci. Rev.* **84**, 239–250 (1998).
60. Ceccarelli, C. et al. in *Protostars and Planets VI* (eds Beuther, H. et al.) 859–882 (Univ. of Arizona Press, 2014).
61. Crovisier, J. et al. The composition of ices in comet C/1995 O1 (Hale–Bopp) from radio spectroscopy. Further results and upper limits on undetected species. *Astron. Astrophys.* **418**, 1141–1157 (2004).

62. Paquette, J. A. et al. D/H in the refractory organics of comet 67P/Churyumov-Gerasimenko measured by Rosetta/COSIMA. *Mon. Not. R. Astron. Soc.* **504**, 4940–4951 (2021).
63. Brown, P. D. & Millar, T. J. Models of the gas–grain interaction – deuterium chemistry. *Mon. Not. R. Astron. Soc.* **237**, 661–671 (1989).

Acknowledgements

The micrometeorites were collected at Concordia Station (Project No. 1120), and their collection was supported by the French Polar Institute (IPEV). We are grateful to IPEV for financial support and to IPEV and National Antarctic Research Program staff for logistical help. This work was financially supported by the French National Agency for Research (Project COMETOR 18-CE31-0011), Région Île-de-France (Major Interest Area ACAV+ under Project C3E), the French National Centre for Space Studies and the French National Centre for Scientific Research (French National Institute for Earth Sciences and Astronomy, the Physics and Chemistry of the Interstellar Medium Program, the National Institute of Nuclear and Particle Physics and the Laboratory of Excellence for Physics of the Two Infinite and of Origins). L.R. thanks the European Research Council for funding (Project HYDROMA under Grant Agreement No. 819587). The NanoSIMS facility in Paris was established by funds from the French National Centre for Scientific Research, Région Île-de-France, Ministère délégué à l'Enseignement Supérieur et à la Recherche, and the Muséum National d'Histoire Naturelle. We acknowledge the CurieCore Tech for the use of Curie-NanoSIMS. J.R. thanks G. Slodzian for his help and precious insights on the NanoSIMS instrument and data treatment.

Author contributions

J.D., E.D. and C.E. conceived and designed the study. J.D., E.D., C.E. and L.D. participated in the fieldwork and the selection of samples. L.D., J.R. and B.G. performed the scanning electron microscopy of the samples. L.R.N., T.-D.W., L.R. and S.M. conceived and performed the NanoSIMS experiments. L.R.N., L.R. and J.D. provided the standards. J.R., N.B. and J.D. participated in the NanoSIMS experiments. R.M.S. performed the focused ion beam microscopy of the samples. J.R. analysed and interpreted the data. J.R., J.D., E.D., C.E., L.R.N., R.M.S. and L.R. wrote the paper.

Competing interests

The authors declare no competing interests.

Additional information

Extended data is available for this paper at https://doi.org/10.1038/s41550-024-02364-y.

Supplementary information The online version contains supplementary material available at https://doi.org/10.1038/s41550-024-02364-y.

Correspondence and requests for materials should be addressed to J. Rojas.

Peer review information *Nature Astronomy* thanks Martin Suttle, Hikaru Yabuta and the other, anonymous, reviewer(s) for their contribution to the peer review of this work.

https://doi.org/10.1038/s41550-024-02364-y

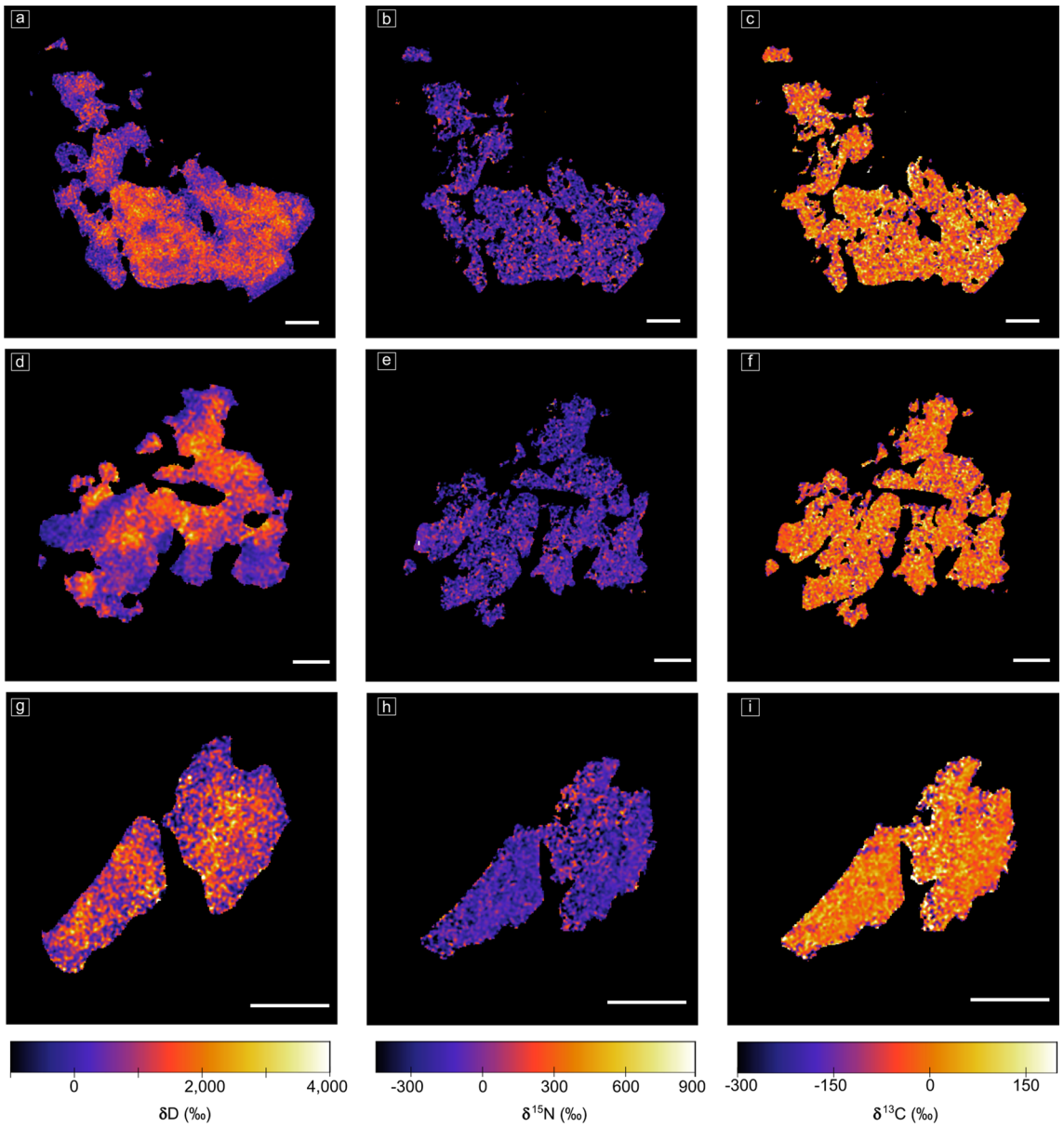

Extended Data Fig. 1 | Isotopic maps of DC06-18. (**a, b, c**) δD, $\delta^{15}N$ and $\delta^{13}C$ maps of the first fragment of DC06-18. (**d, e, f**) δD, $\delta^{15}N$ and $\delta^{13}C$ maps of the second fragment of DC06-18. (**g, h, i**) δD, $\delta^{15}N$ and $\delta^{13}C$ maps of the third fragment of DC06-18. The white scale bar is 5 μm.

https://doi.org/10.1038/s41550-024-02364-y

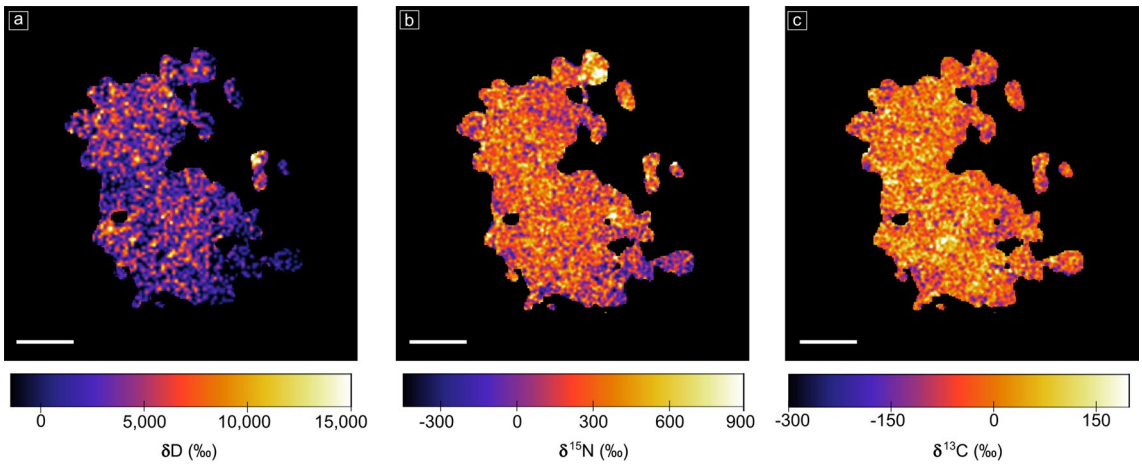

Extended Data Fig. 2 | Isotopic maps of DC06-43. (**a, b, c**) δD, δ^{15}N and δ^{13}C maps. The white scale bar is 2 µm.

https://doi.org/10.1038/s41550-024-02364-y

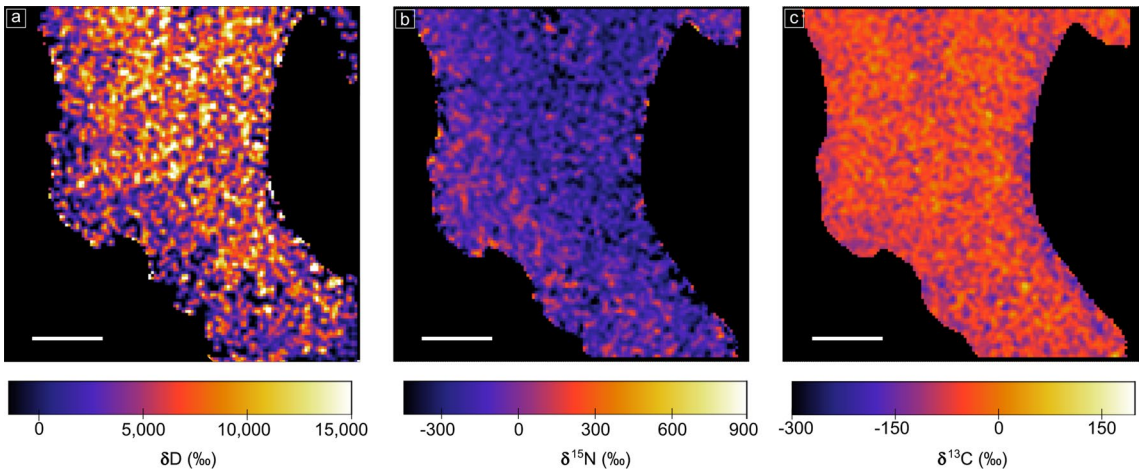

Extended Data Fig. 3 | Isotopic maps of DC16-309. (**a, b, c**) δD, $\delta^{15}N$ and $\delta^{13}C$ maps. The white scale bar is 1 µm.

https://doi.org/10.1038/s41550-024-02364-y

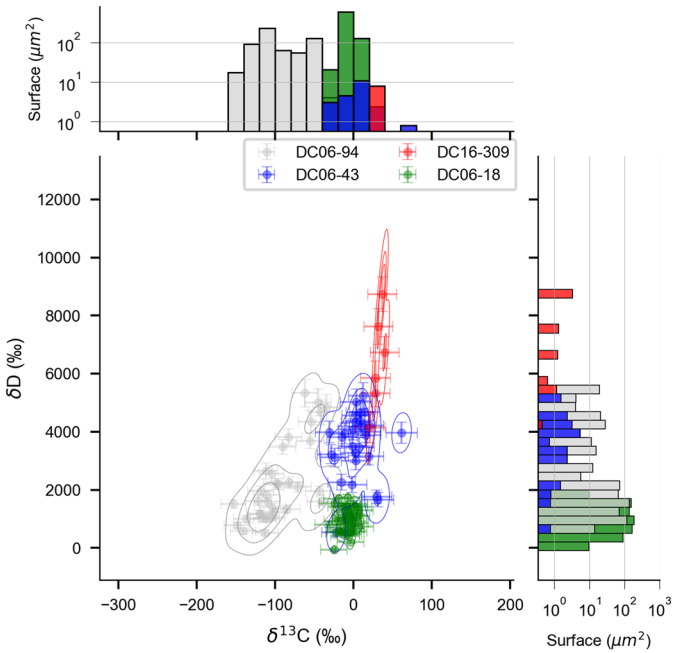

Extended Data Fig. 4 | δ^{13}C versus δD isotopic composition of the 4 UCAMMs presented in this paper. DC06-94, DC06-43, DC06-18 and DC16-309 are plotted in gray, blue, green, and red, respectively. Histograms in the margins indicate the analyzed area in µm² (in log scale). Data points are the mean isotopic ratios measured in individual regions of interest +/- one standard deviation (Methods-Data reduction and Supplementary Table). Isodensity contours of the density functions at 5% (threshold), 33% and 66% are displayed by the solid lines.

https://doi.org/10.1038/s41550-024-02364-y

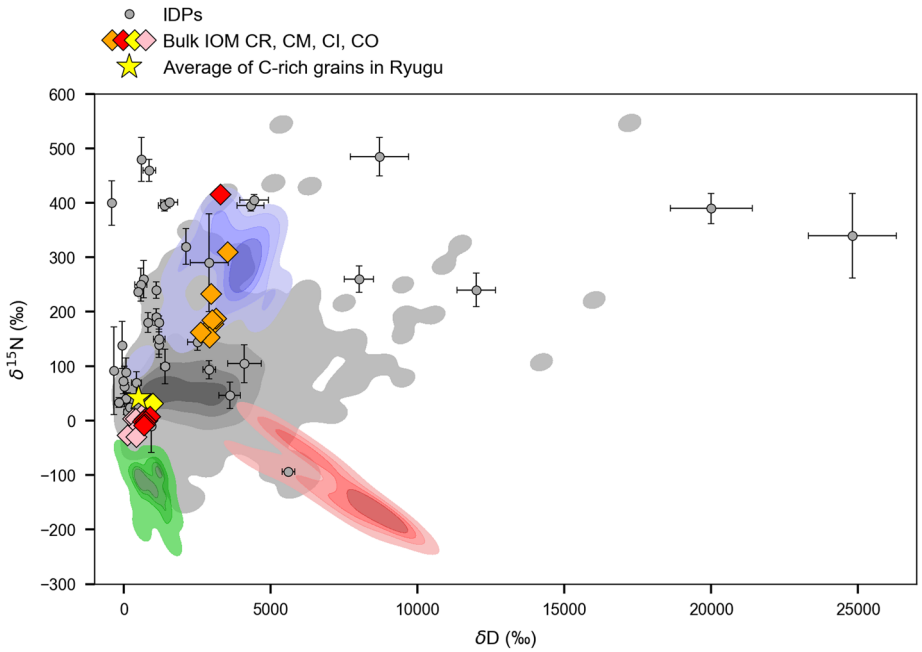

Extended Data Fig. 5 | Comparison of the H and N isotopic compositions measured in UCAMMs with literature data. DC06-94, DC06-43, DC06-18 and DC16-309 are displayed with gray, blue, green, and red contours, respectively. Literature data for IDPs[10,14,15] are plotted with gray dots. IOM of CR, CM, CI and CO chondrites[1] are plotted with orange, red, yellow and pink diamonds, respectively. The bulk Ryugu composition[18] is displayed by the yellow star. Error bars are one standard deviation.

https://doi.org/10.1038/s41550-024-02364-y

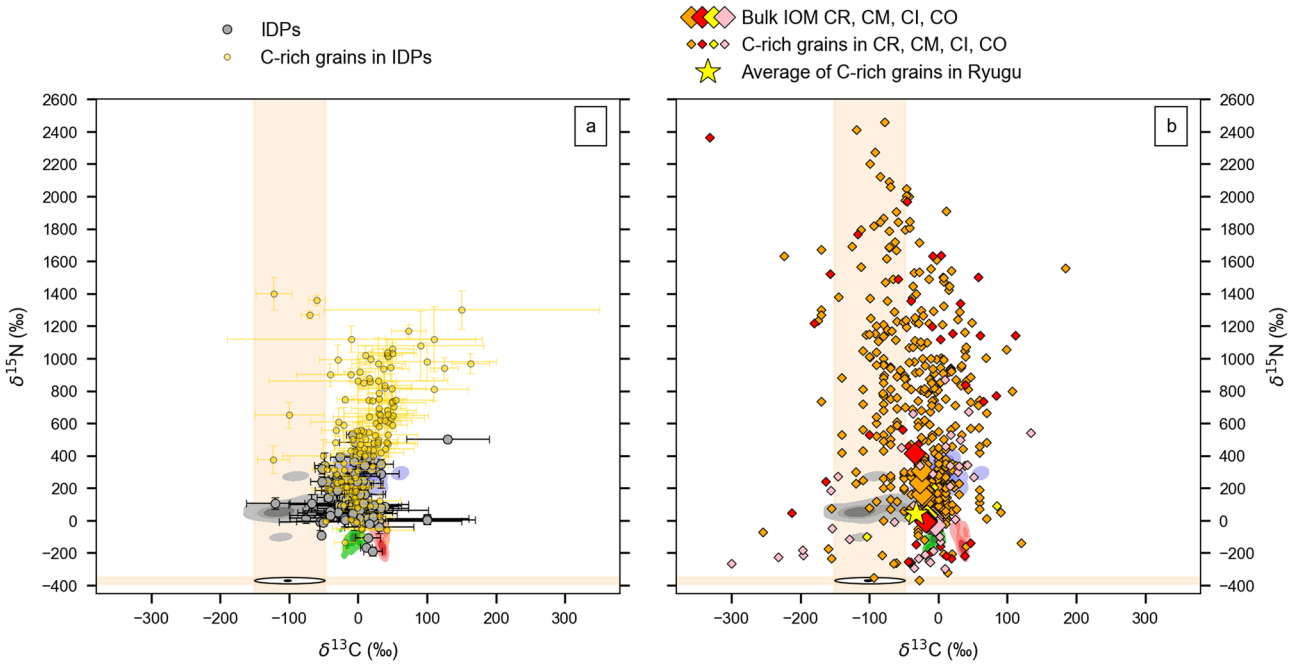

Extended Data Fig. 6 | Comparison of the C and N isotopic composition of the 4 analyzed UCAMMs with literature data. (**a, b**) DC06-94, DC06-43, DC06-18 and DC16-309 are in gray, blue, green and red contours. Literature data for IDPs (a) and carbonaceous matter from meteorites (b) are superimposed. Bulk IDPs[10–15] and hotspots in IDPs[11–14] are indicated in the panel a) as dark gray dots and yellow dots with one standard deviation error bars. Bulk IOM data are indicated as large diamonds in orange (CR), red (CM), yellow (CI) and pink (CO)[1]. Carbonaceous grains in CR, CM, CI and CO[3,5–9] are indicated as small diamonds with the same color code. The average composition of carbonaceous asteroid Ryugu grains[18] from the Hayabusa2 JAXA return sample mission is reported as a yellow star. The shaded area and the ellipse represent the range of variation of the solar $\delta^{15}N$ and $\delta^{13}C$ value.

https://doi.org/10.1038/s41550-024-02364-y

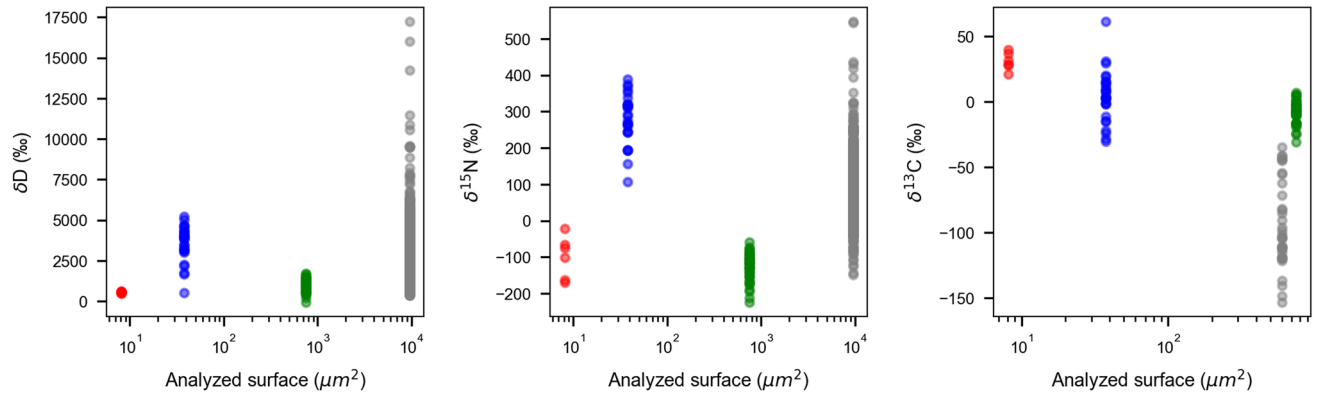

Extended Data Fig. 7 | H (left), N (middle) and C (right) isotopic compositions of the 4 UCAMMs plotted against their analyzed surfaces. Red: DC16-309; blue: DC06-43; green: DC06-18; gray: DC06-94.

https://doi.org/10.1038/s41550-024-02364-y

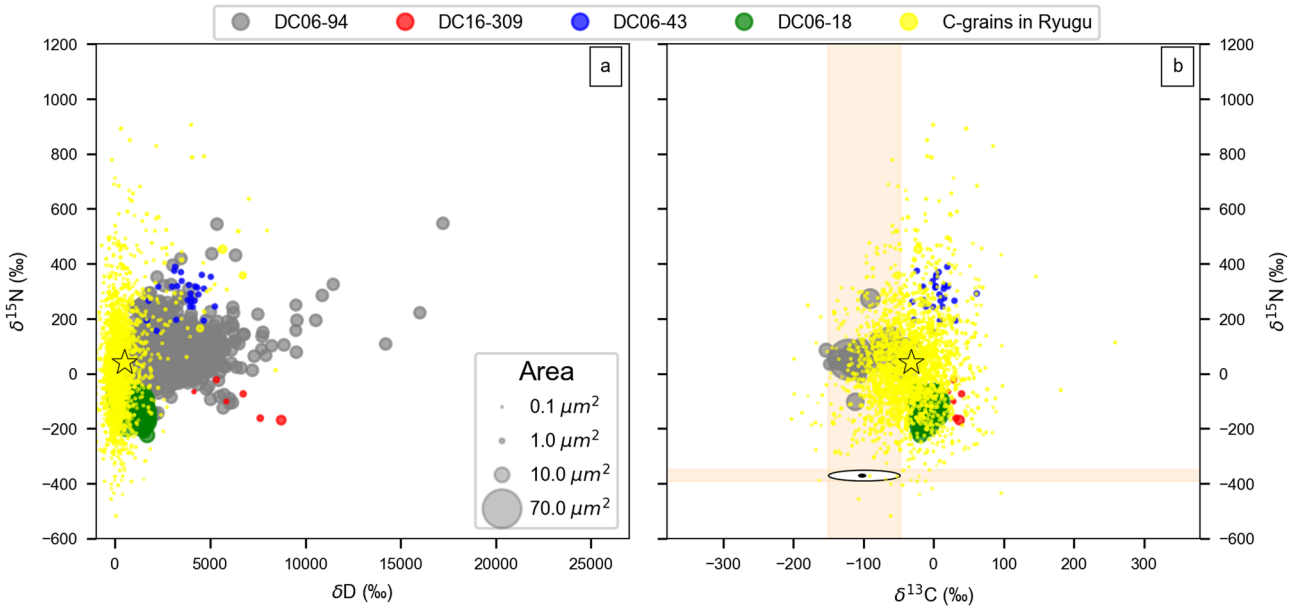

Extended Data Fig. 8 | Comparison of the H, C and N isotopic composition of UCAMMs and Ryugu grains. (**a**) N and H isotopic compositions. (**b**) N and C isotopic compositions. UCAMMs are displayed with grey, red, blue, and green circles. Ryugu samples[18] are plotted with yellow circles. The size of the circles indicates the size of the measured ROIs in UCAMMs and Ryugu grains. The bulk composition of the C-rich particles in Ryugu grains is displayed by a star. The distinct N and C isotopic compositions evidenced in UCAMMs are observed at small scale in Ryugu grains.

https://doi.org/10.1038/s41550-024-02364-y

Extended Data Table 1 | Characteristics of the NanoSIMS acquisitions

UCAMMs	Area (µm²)	Session H		Session N		Session C		
		Raster (pixels)	# frames	Raster (pixels)	# frames	Sub-area (µm²)	Raster (pixels)	# frames
DC06-94 Z1	50x50	512x512	87	512x512	158	20x20	256x256	200
DC06-94 Z2	50x50	512x512	79	512x512	30	20x20	256x256	200
DC06-94 Z3	50x50	512x512	124	512x512	30			
DC06-94 Z4	50x50	512x512	80	512x512	120	20x20	256x256	200
DC06-94 Z5	50x50	512x512	119	512x512	118			
DC06-94 Z6	50x50	512x512	30	512x512	160	20x20	256x256	200

		Session H		Session C & N	
		Raster (pixels)	# frames	Raster (pixels)	# frames
DC16-309	5x5	128x128	15	128x128	20
DC06-43	12x12	128x128	26	256x256	10
DC06-18 A	50x50	512x512	30	512x512	35
DC06-18 B	45x45	256x256	40	512x512	30
DC06-18 C	20x20	256x256	11	256x256	30